Spline-contoured Radome Synthesis via System-by-Design

M. Salucci, G. Oliveri, M. A. Hannan and A. Massa

Contents

1 [APPROACH 1] Optimization with PSO + Kriging (no update during optimization) - EXP CORRELATION

1.0.1 Goal

This section is aimed at showing the results of the optimization carried out with

- Optimizer: Particle Swarm Optimization (PSO)
- Predictor: Kriging

During the optimization, **no update of the training set will be done**. The optimization will use always the same trained model to predict the fitness of each particle until the last iteration is reached.

1.0.2 Parameters

Optimization targets

- Number of variables: $K = 5$;
- Frequency range:
  - Minimum frequency: $f_{min} = 10.75$ $[GHz]$;
  - Maximum frequency: $f_{max} = 14.5$ $[GHz]$;
  - Number of frequency steps: $N_f = 10$ ($\Delta f \simeq 0.42$ $[GHz]$);
  - Central frequency: $f_0 = \frac{f_{min}+f_{max}}{2} \simeq 12.63$ $[GHz]$;
  - Free-space wavelength at the central frequency: $\lambda_0 = \frac{c}{f_0} = 2.38 \times 10^{-2}$ $[m]$;
- Scanning angle range:
  - Minimum scanning angle: $\theta_{min} = 0$ $[deg]$;
  - Maximum scanning angle: $\theta_{max} = 45$ $[deg]$;
  - Number of angular steps: $N_\theta = 4$ ($\theta_1 = 0$ $[deg]$, $\theta_2 = 15$ $[deg]$, $\theta_3 = 30$ $[deg]$, $\theta_4 = 45$ $[deg]$);

PSO **parameters**

- Population dimension: $P = 10$;
- Maximum number of iterations: $I_{max} = 200$;
- Fitness threshold: $\Phi^{th} = 10^{-20}$;
- Inertial weight: $w = 0.4$;
- Constant inertial velocity;
- Exploration coefficient: $c_1 = 2$;
- Exploitation coefficient: $c_2 = 2$;
- Random seed $s = 1, 2, ..., 10$;
- Initialization (generation of the initial swarm): use the same seed for all the optimizations.

Kriging (Gaussian Process Regressor) parameters

- Regression model: constant (Ordinary Kriging);
- Correlation models:
  - Exponential ($p = 1$);

- Initial guess for hyper-parameters θ_h: $\theta_{h,0} = 0.5$, for $h = 1, ..., K$;
- Lower bound for hyper-parameters θ_h: $min\,\{\theta_h\} = 0.1$, for $h = 1, ..., K$;
- Upper bound for hyper-parameters θ_h: $max\,\{\theta_h\} = 20.0$, for $h = 1, ..., K$.

Not-optimized (static) radome parameter

Parameter	Description	Value
L	Length of the radome	1.59×10^{-1} $[m] \simeq 6.69\ \lambda_0$
D	Base diameter of the radome	1.27×10^{-1} $[m] \simeq 5.35\ \lambda_0$
t_0	Thickness of the base and of the top of the radome	$8.20 \times 10^{-3}[m] \simeq \frac{\lambda_r}{2}$
z_1	z-coordinate of the spline control point 1	$\frac{L-t_0}{6}$
z_2	z-coordinate of the spline control point 2	$2\frac{L-t_0}{6}$
z_3	z-coordinate of the spline control point 3	$3\frac{L-t_0}{6}$
z_4	z-coordinate of the spline control point 4	$4\frac{L-t_0}{6}$
z_5	z-coordinate of the spline control point 5	$5\frac{L-t_0}{6}$
ν	External curvature of the radome ($\nu \in [1, 2]$)	1.449 (tangent ogive)
ε_r	Permittivity of the radome material	2.10 (Teflon)
$\tan\delta_r$	Tangent delta of the radome material	$tan\delta = 3.00 \times 10^{-4}$ @ 10.0 $[GHz]$ (Teflon)
λ_r	Wavelength in the radome material	$\lambda_r \simeq \frac{c}{f_0\sqrt{\varepsilon}} \simeq 1.64 \times 10^{-1}$

Table I: List of non-optimized radome parameters.

Antenna Parameters

- Linear dipole array placed over circular ground plane (PEC)
- Number of array elements: $N_e = 8$
- Dipole length: $l_e = \frac{\lambda_0}{2}$
- Array elements spacing: $d_e = \lambda/2$
- Spacing between the array and the ground plane: $h_e = \frac{\lambda_0}{4}$

Parameters boundaries

Parameter	Description	Min	Max
t_1	Radome thickness at the quota $z = z_1$	3.28×10^{-3}[m] $(0.2\lambda_r)$	13.12×10^{-3}[m] $(0.8\lambda_r)$
t_2	Radome thickness at the quota $z = z_2$	3.28×10^{-3}[m] $(0.2\lambda_r)$	13.12×10^{-3}[m] $(0.8\lambda_r)$
t_3	Radome thickness at the quota $z = z_3$	3.28×10^{-3}[m] $(0.2\lambda_r)$	13.12×10^{-3}[m] $(0.8\lambda_r)$
t_4	Radome thickness at the quota $z = z_4$	3.28×10^{-3}[m] $(0.2\lambda_r)$	13.12×10^{-3}[m] $(0.8\lambda_r)$
t_5	Radome thickness at the quota $z = z_5$	3.28×10^{-3}[m] $(0.2\lambda_r)$	13.12×10^{-3}[m] $(0.8\lambda_r)$

Table II: List of all considered boundaries for the optimized radome descriptors.

1.0.3 Predicted fitness vs. iteration index ($s \in [1, 10]$)

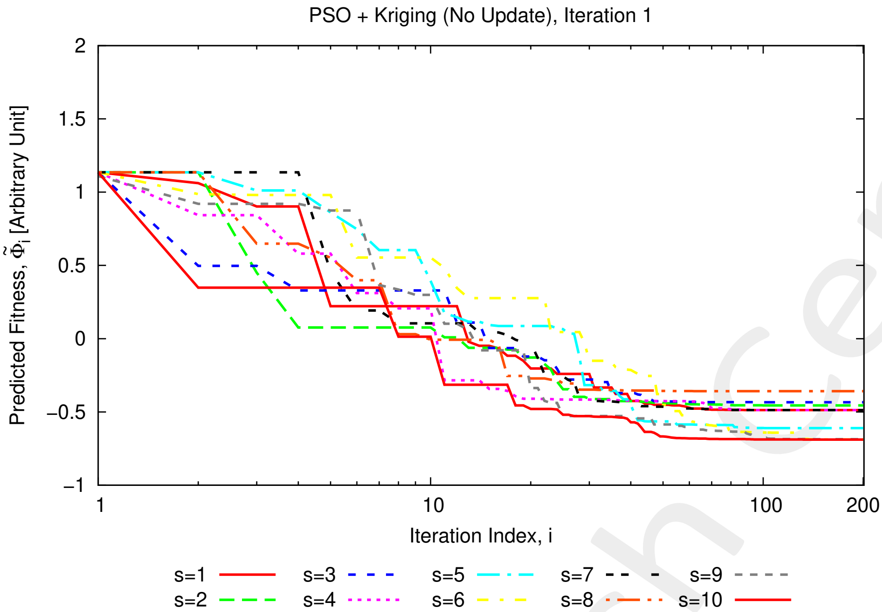

Figure 1: Predicted fitness vs. iteration index, for different random seeds ($s \in [1, 10]$).

1.0.4 Predicted fitness vs. real fitness

Legend

- $\widetilde{\Phi}_0$: Predicted fitness for the best particle of the initial swarm;
- Φ_0: Actual fitness for the best particle of the initial swarm;
- $\widetilde{\Phi}^{opt}$: Predicted fitness for the optimal solution found at the end of the PSO;
- Φ^{opt}: Actual fitness computed for the optimal solution found at the end of the PSO;
- $\Phi^{opt}_{train} = 1.13$: Best fitness inside the training set at current iteration.

	Predicted		Actual		
Seed (s)	$\widetilde{\Phi}_0$	$\widetilde{\Phi}^{opt}$	Φ_0	Φ^{opt}	$100\frac{\Phi^{opt}_{train}-\Phi^{opt}}{\Phi^{opt}_{train}}$
1	1.13	-4.88×10^{-1}	2.11	1.62	−43.36
2	1.13	-4.55×10^{-1}	2.11	1.45	−28.32
3	1.13	-4.33×10^{-1}	2.11	1.19	−5.31
4	1.13	-4.88×10^{-1}	2.11	1.62	−43.36
5	1.13	-6.11×10^{-1}	2.11	1.53	−35.40
6	1.13	-6.88×10^{-1}	2.11	1.32	−16.81
7	1.13	-4.88×10^{-1}	2.11	1.62	−43.36
8	**1.13**	$\mathbf{-3.58 \times 10^{-1}}$	**2.11**	**1.07**	**5.31**
9	1.13	-6.86×10^{-1}	2.11	1.33	−17.70
10	1.13	-6.88×10^{-1}	2.11	1.32	−16.81

Table III: Number of updates during the optimization, initial and final predicted fitness and associated real fitness, for each considered random seed $s \in [1, 10]$.

Statistics (over $S = 10$ seeds)

Predicted				Actual			
$min\left\{\widetilde{\Phi}^{opt}\right\}$	$max\left\{\widetilde{\Phi}^{opt}\right\}$	$avg\left\{\widetilde{\Phi}^{opt}\right\}$	$std\left\{\widetilde{\Phi}^{opt}\right\}$	$min\left\{\Phi^{opt}\right\}$	$max\left\{\Phi^{opt}\right\}$	$avg\left\{\Phi^{opt}\right\}$	$std\left\{\Phi^{opt}\right\}$
-6.88×10^{-1}	-3.58×10^{-1}	-5.38×10^{-1}	1.14×10^{-1}	1.07	1.62	1.41	1.84×10^{-1}

Table IV: Statistics (min, max, average and standard deviation) of the predicted and actual fitness obtained over $S = 10$ seeds.

Difference between predicted and actual fitness

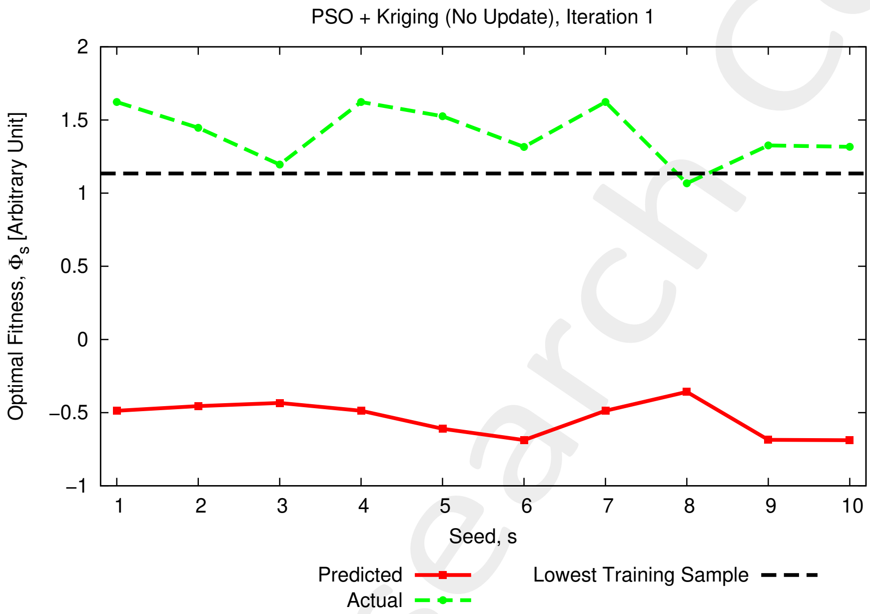

Figure 2: Predicted and actual final fitness for different random seeds ($s \in [1, 10]$).

- Mean Absolute Error (MAE): $MAE = \frac{1}{S}\sum_{s=1}^{S}\left|\widetilde{\Phi}_s^{opt} - \Phi_s^{opt}\right|$
- Normalized Mean Error (NME): $NME = \frac{1}{S}\sum_{s=1}^{S}\frac{\left|\widetilde{\Phi}_s^{opt} - \Phi_s^{opt}\right|}{\left|\Phi_s^{opt}\right|}$
- Matching Error (ME): $ME = \frac{1}{S}\frac{\sum_{s=1}^{S}\left|\widetilde{\Phi}_s^{opt} - \Phi_s^{opt}\right|^2}{\sum_{s=1}^{S}\left|\Phi_s^{opt}\right|^2}$

MAE	NME	ME
1.94	1.39	1.90

Table V: Difference between final predicted and actual fitness for all the considered random seeds.

1.0.5 Optimized parameters $(t_1^{opt}, ..., t_5^{opt})$ vs. seed

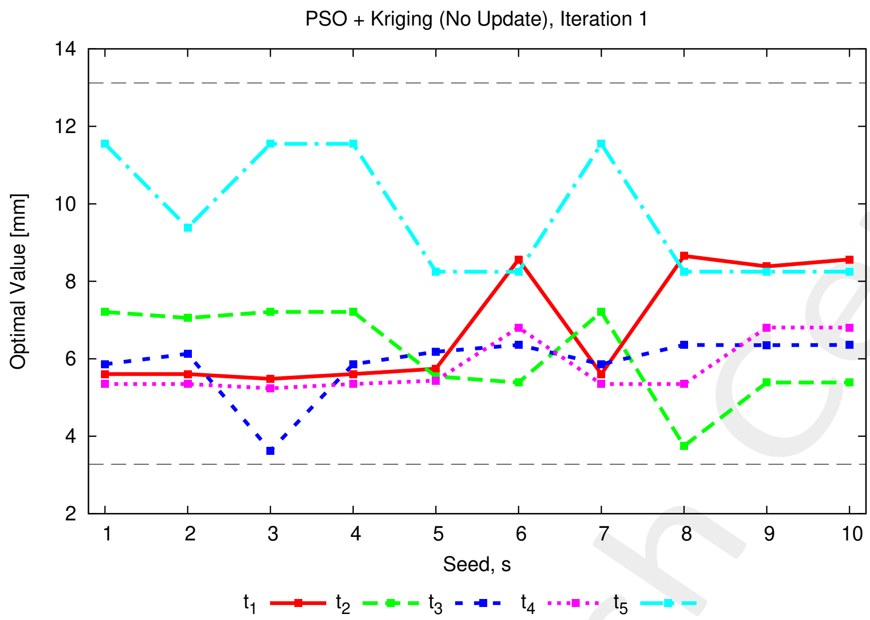

Figure 3: Optimized value of each spline control point for the analyzed seeds.

1.0.6 Best solution found (min. actual fitness)

Seed: $s = 8$;

- True fitness: $\Phi^{opt} = 1.07$;
- Average BSE error: $BSE_{avg} = \sqrt{\Phi^{opt}} = 1.03$ [deg].

1.0.7 Observations

- All the considered random seeds ended with a **negative predicted fitness**;
- in the next section, the same optimizations will be re-executed by updating the training set when the predicted fitness of a given particle is negative during the PSO optimization.

2 [APPROACH 1] Optimization with PSO + Kriging (no update during optimization) - GAUSS CORRELATION

2.0.1 Parameters

Optimization targets

- Number of variables: $K = 5$;
- Frequency range:
  - Minimum frequency: $f_{min} = 10.75$ $[GHz]$;
  - Maximum frequency: $f_{max} = 14.5$ $[GHz]$;
  - Number of frequency steps: $N_f = 10$ ($\Delta f \simeq 0.42$ $[GHz]$);
  - Central frequency: $f_0 = \frac{f_{min}+f_{max}}{2} \simeq 12.63$ $[GHz]$;
  - Free-space wavelength at the central frequency: $\lambda_0 = \frac{c}{f_0} = 2.38 \times 10^{-2}$ $[m]$;
- Scanning angle range:
  - Minimum scanning angle: $\theta_{min} = 0$ $[deg]$;
  - Maximum scanning angle: $\theta_{max} = 45$ $[deg]$;
  - Number of angular steps: $N_\theta = 4$ ($\theta_1 = 0$ $[deg]$, $\theta_2 = 15$ $[deg]$, $\theta_3 = 30$ $[deg]$, $\theta_4 = 45$ $[deg]$);

PSO **parameters**

- Population dimension: $P = 10$;
- Maximum number of iterations: $I_{max} = 200$;
- Fitness threshold: $\Phi^{th} = 10^{-20}$;
- Inertial weight: $w = 0.4$;
- Constant inertial velocity;
- Exploration coefficient: $c_1 = 2$;
- Exploitation coefficient: $c_2 = 2$;
- Random seed $s = 1, 2, ..., 10$;
- Initialization (generation of the initial swarm): use the same seed for all the optimizations.

Kriging (Gaussian Process Regressor) parameters

- Regression model: constant (Ordinary Kriging);

- Correlation models:
  - **Gaussian ($p = 2$);**
- Initial guess for hyper-parameters θ_h: $\theta_{h,0} = 0.5$, for $h = 1, ..., K$;
- Lower bound for hyper-parameters θ_h: $min\{\theta_h\} = 0.1$, for $h = 1, ..., K$;
- Upper bound for hyper-parameters θ_h: $max\{\theta_h\} = 20.0$, for $h = 1, ..., K$.

Not-optimized (static) radome parameter

Parameter	**Description**	**Value**
L	Length of the radome	1.59×10^{-1} $[m] \simeq 6.69\ \lambda_0$
D	Base diameter of the radome	1.27×10^{-1} $[m] \simeq 5.35\ \lambda_0$
t_0	Thickness of the base and of the top of the radome	$8.20 \times 10^{-3}[m] \simeq \frac{\lambda_r}{2}$
z_1	z-coordinate of the spline control point 1	$\frac{L-t_0}{6}$
z_2	z-coordinate of the spline control point 2	$2\frac{L-t_0}{6}$
z_3	z-coordinate of the spline control point 3	$3\frac{L-t_0}{6}$
z_4	z-coordinate of the spline control point 4	$4\frac{L-t_0}{6}$
z_5	z-coordinate of the spline control point 5	$5\frac{L-t_0}{6}$
ν	External curvature of the radome ($\nu \in [1, 2]$)	1.449 (tangent ogive)
ε_r	Permittivity of the radome material	2.10 (Teflon)
tanδ_r	Tangent delta of the radome material	$tan\delta = 3.00 \times 10^{-4}$ @ 10.0 $[GHz]$ (Teflon)
λ_r	Wavelength in the radome material	$\lambda_r \simeq \frac{c}{f_0\sqrt{\varepsilon}} \simeq 1.64 \times 10^{-1}$

Table VI: List of non-optimized radome parameters.

Antenna Parameters

- Linear dipole array placed over circular ground plane (PEC)
- Number of array elements: $N_e = 8$
- Dipole length: $l_e = \frac{\lambda_0}{2}$
- Array elements spacing: $d_e = \lambda/2$
- Spacing between the array and the ground plane: $h_e = \frac{\lambda_0}{4}$

Parameters boundaries

Parameter	**Description**	Min	Max
t_1	Radome thickness at the quota $z = z_1$	3.28×10^{-3}[m] $(0.2\lambda_r)$	13.12×10^{-3}[m] $(0.8\lambda_r)$
t_2	Radome thickness at the quota $z = z_2$	3.28×10^{-3}[m] $(0.2\lambda_r)$	13.12×10^{-3}[m] $(0.8\lambda_r)$
t_3	Radome thickness at the quota $z = z_3$	3.28×10^{-3}[m] $(0.2\lambda_r)$	13.12×10^{-3}[m] $(0.8\lambda_r)$
t_4	Radome thickness at the quota $z = z_4$	3.28×10^{-3}[m] $(0.2\lambda_r)$	13.12×10^{-3}[m] $(0.8\lambda_r)$
t_5	Radome thickness at the quota $z = z_5$	3.28×10^{-3}[m] $(0.2\lambda_r)$	13.12×10^{-3}[m] $(0.8\lambda_r)$

Table VII: List of all considered boundaries for the optimized radome descriptors.

2.0.2 Predicted fitness vs. iteration index ($s \in [1, 10]$)

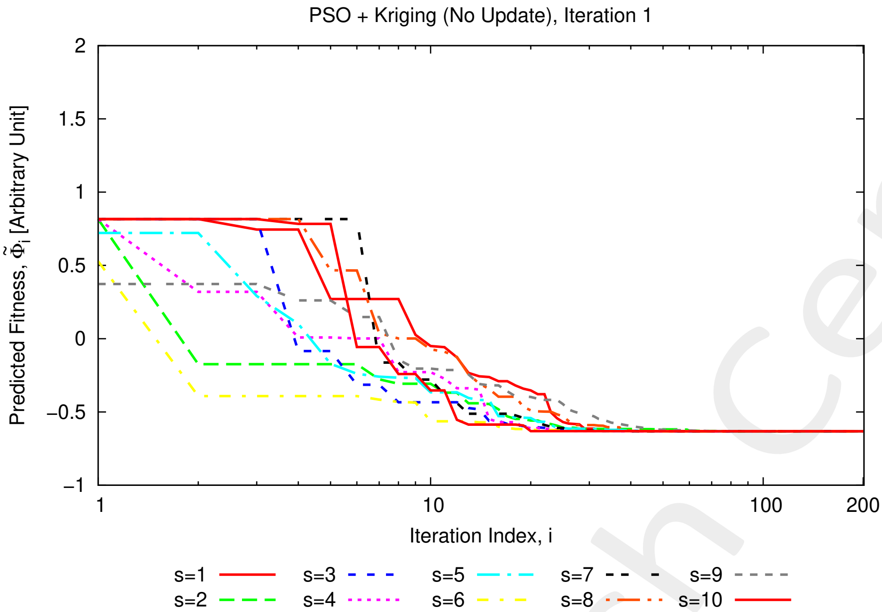

Figure 4: Predicted fitness vs. iteration index, for different random seeds ($s \in [1, 10]$).

2.0.3 Predicted fitness vs. real fitness

Legend

- $\widetilde{\Phi}_0$: Predicted fitness for the best particle of the initial swarm;
- Φ_0: Actual fitness for the best particle of the initial swarm;
- $\widetilde{\Phi}^{opt}$: Predicted fitness for the optimal solution found at the end of the PSO;
- Φ^{opt}: Actual fitness computed for the optimal solution found at the end of the PSO;
- $\Phi^{opt}_{train} = 1.13$: Best fitness inside the training set at current iteration.

	Predicted		**Actual**		
Seed (s)	$\widetilde{\Phi}_0$	$\widetilde{\Phi}^{opt}$	Φ_0	Φ^{opt}	$100\frac{\Phi^{opt}_{train}-\Phi^{opt}}{\Phi^{opt}_{train}}$
1	8.16×10^{-1}	-6.31×10^{-1}	2.11	1.19	-5.31
2	8.16×10^{-1}	-6.31×10^{-1}	2.11	1.19	-5.31
3	$\mathbf{8.16 \times 10^{-1}}$	$\mathbf{-6.31 \times 10^{-1}}$	**2.11**	**1.18**	$\mathbf{-4.42}$
4	8.16×10^{-1}	-6.31×10^{-1}	2.11	1.19	-5.31
5	8.16×10^{-1}	-6.31×10^{-1}	2.11	1.19	-5.31
6	8.16×10^{-1}	-6.31×10^{-1}	2.11	1.19	-5.31
7	8.16×10^{-1}	-6.31×10^{-1}	2.11	1.19	-5.31
8	8.16×10^{-1}	-6.31×10^{-1}	2.11	1.19	-5.31
9	8.16×10^{-1}	-6.31×10^{-1}	2.11	1.19	-5.31
10	8.16×10^{-1}	-6.31×10^{-1}	2.11	1.19	-5.31

Table VIII: Number of updates during the optimization, initial and final predicted fitness and associated real fitness, for each considered random seed $s \in [1, 10]$.

Statistics (over $S = 10$ seeds)

Predicted				Actual			
$min\left\{\widetilde{\Phi}^{opt}\right\}$	$max\left\{\widetilde{\Phi}^{opt}\right\}$	$avg\left\{\widetilde{\Phi}^{opt}\right\}$	$std\left\{\widetilde{\Phi}^{opt}\right\}$	$min\left\{\Phi^{opt}\right\}$	$max\left\{\Phi^{opt}\right\}$	$avg\left\{\Phi^{opt}\right\}$	$std\left\{\Phi^{opt}\right\}$
-6.31×10^{-1}	-6.31×10^{-1}	-6.31×10^{-1}	0	1.18	1.19	1.19	2.4×10^{-3}

Table IX: Statistics (min, max, average and standard deviation) of the predicted and actual fitness obtained over $S = 10$ seeds.

Difference between predicted and actual fitness

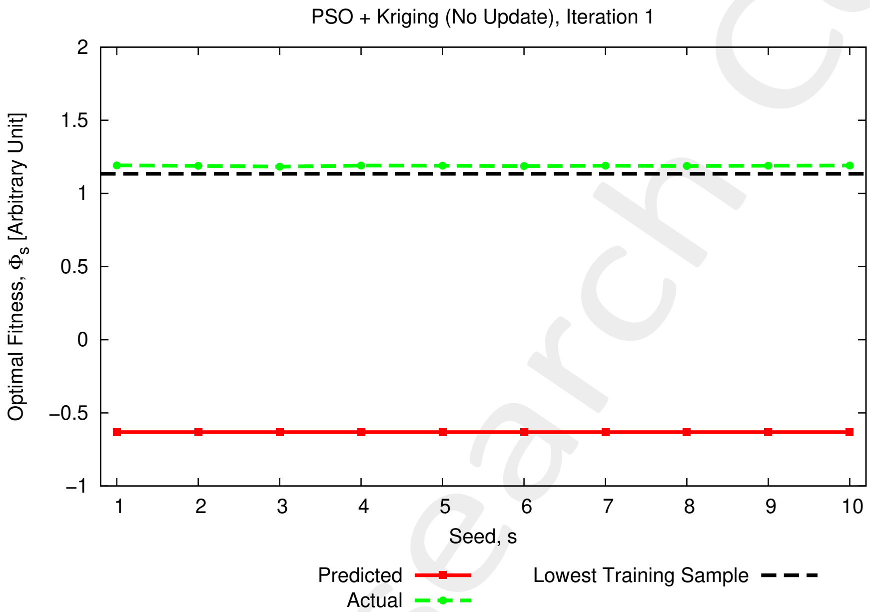

Figure 5: Predicted and actual final fitness for different random seeds ($s \in [1, 10]$).

- Mean Absolute Error (MAE): $MAE = \frac{1}{S}\sum_{s=1}^{S}\left|\widetilde{\Phi}_s^{opt} - \Phi_s^{opt}\right|$
- Normalized Mean Error (NME): $NME = \frac{1}{S}\sum_{s=1}^{S}\frac{\left|\widetilde{\Phi}_s^{opt} - \Phi_s^{opt}\right|}{\left|\Phi_s^{opt}\right|}$
- Matching Error (ME): $ME = \frac{1}{S}\frac{\sum_{s=1}^{S}\left|\widetilde{\Phi}_s^{opt} - \Phi_s^{opt}\right|^2}{\sum_{s=1}^{S}\left|\Phi_s^{opt}\right|^2}$

MAE	NME	ME
1.82	1.53	2.34

Table X: Difference between final predicted and actual fitness for all the considered random seeds.

2.0.4 Optimized parameters $(t_1^{opt}, ..., t_5^{opt})$ vs. seed

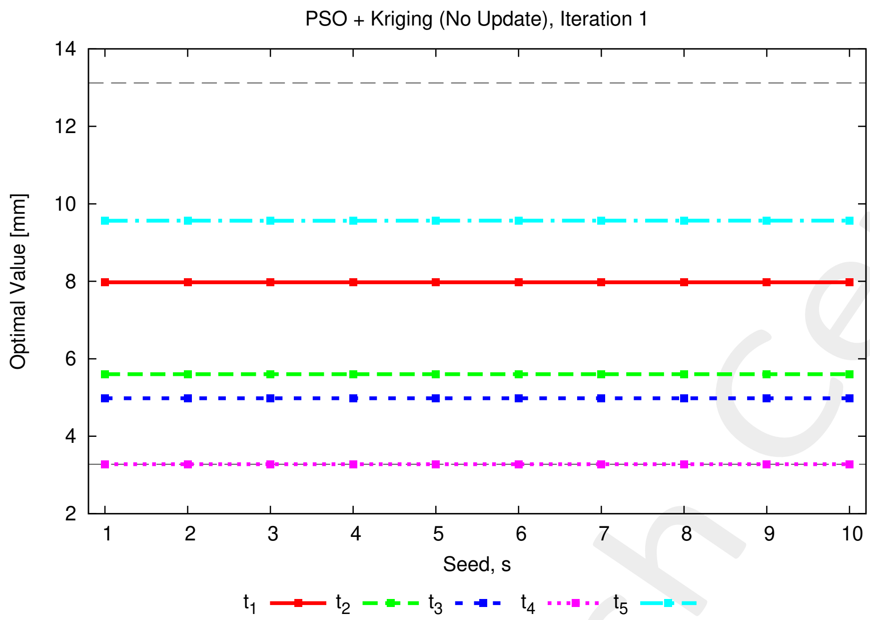

Figure 6: Optimized value of each spline control point for the analyzed seeds.

2.0.5 Best solution found (min. actual fitness)

- Seed: $s = 3$;
- True fitness: $\Phi^{opt} = 1.18$;
- Average BSE error: $BSE_{avg} = \sqrt{\Phi^{opt}} = 1.09$ [deg].

2.0.6 Observations

- All the considered random seeds ended with a **negative predicted fitness,** even with the Gaussian correlation model.

2.0.7 Analysis of the best solution (seed $s = 3$)

Fitness evolution

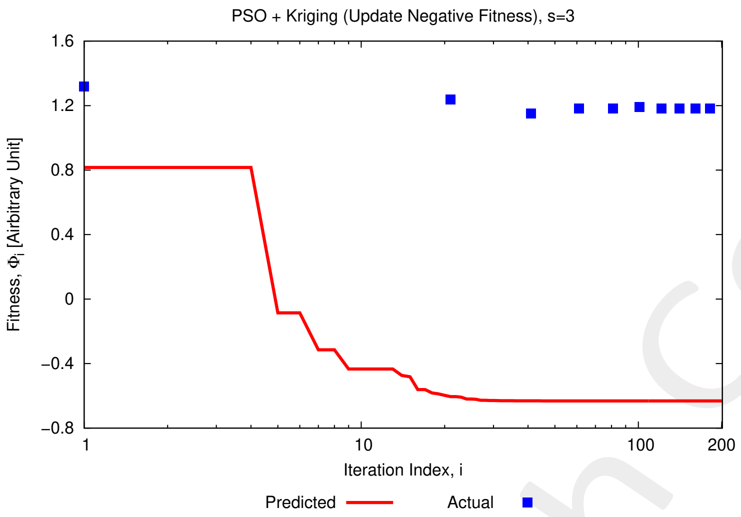

Figure 7: Evolution of the (predicted) fitness and actual fitness computed for the intermediate optimal particles each 20 iterations ("control points").

Optimized parameters ($t_1^{opt}, ..., t_5^{opt}$)

Parameter	**Description**	**Optimized Value [m]**	Min [m]	Max [m]
t_1	Radome thickness at the quota $z = z_1$	7.98×10^{-3}	3.28×10^{-3}	13.12×10^{-3}
t_2	Radome thickness at the quota $z = z_2$	5.60×10^{-3}	3.28×10^{-3}	13.12×10^{-3}
t_3	Radome thickness at the quota $z = z_3$	4.98×10^{-3}	3.28×10^{-3}	13.12×10^{-3}
t_4	Radome thickness at the quota $z = z_4$	3.28×10^{-3}	3.28×10^{-3}	13.12×10^{-3}
t_5	Radome thickness at the quota $z = z_5$	9.56×10^{-3}	3.28×10^{-3}	13.12×10^{-3}

Table XI: Optimized parameters for the best seed ($s = 3$).

Pointing error (BSE) vs. frequency

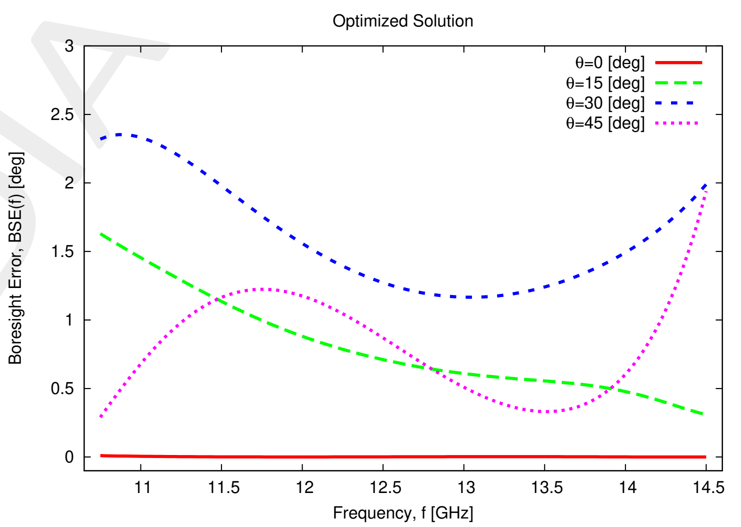

Figure 8: Pointing error (BSE) vs. frequency.

Directivity patterns

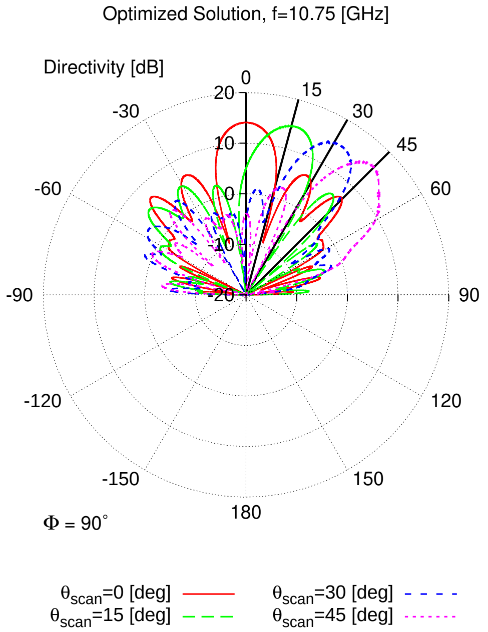

(a) $f = 10.75$ [GHz]

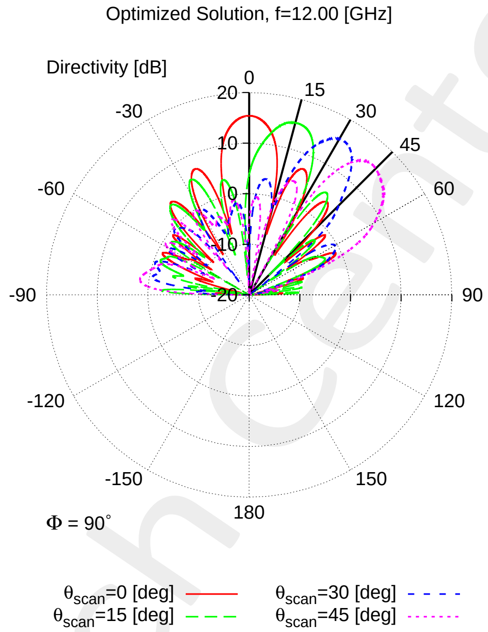

(b) $f = 12.00$ [GHz]

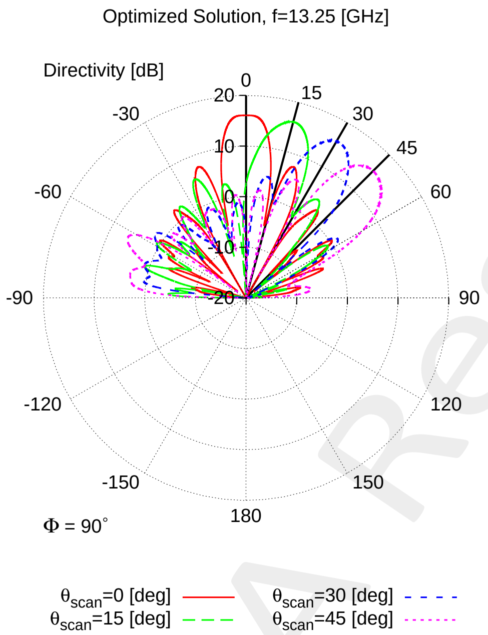

(c) $f = 13.25$ [GHz]

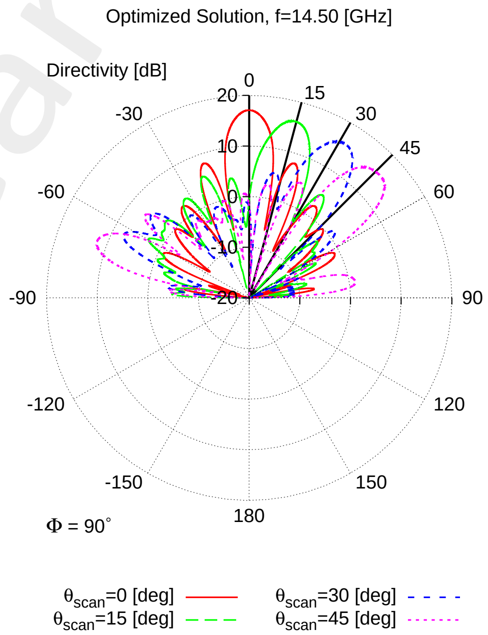

(d) $f = 14.50$ [GHz]

Figure 9: Radiated pattern for the optimized solution at (a) 10.75 [GHz], (b) 12.00 [GHz], (c) 13.25 [GHz] and (d) 14.50 [GHz].

More information on the topics of this document can be found in the following list of references.

References

[1] A. Massa, D. Marcantonio, X. Chen, M. Li, and M. Salucci, "DNNs as applied to electromagnetics, antennas, and propagation - A review," *IEEE Antennas and Wirel. Propag. Lett.,* vol. 18, no. 11, pp. 2225-2229, Nov. 2019.

[2] A. Massa, G. Oliveri, M. Salucci, N. Anselmi, and P. Rocca, "Learning-by-examples techniques as applied to electromagnetics," *Journal of Electromagnetic Waves and Applications, Invited Review Article*, pp. 1-16, 2017.

[3] G. Oliveri, M. Salucci, and A. Massa, "Towards reflectarray digital twins - An EM-driven machine learning perspective," *IEEE Trans. Antennas Propag. - Special Issue on 'Machine Learning in Antenna Design, Modeling, and Measurements*', vol. 70, no. 7, pp. 5078-5093, July 2022.

[4] M. Salucci, L. Tenuti, G. Oliveri, and A. Massa, "Efficient prediction of the EM response of reflectarray antenna elements by an advanced statistical learning method," *IEEE Trans. Antennas Propag.*, vol. 66, no. 8, pp. 3995-4007, Aug. 2018.

[5] M. Salucci, G. Oliveri, M. A. Hannan, and A. Massa, "System-by-design paradigm-based synthesis of complex systems: The case of spline-contoured 3D radomes," *IEEE Antennas and Propagation Magazine - Special Issue on 'Artificial Intelligence in Electromagnetics,*', vol. 64, no. 1, pp. 72-83, Feb. 2022.

[6] G. Oliveri, P. Rocca, M. Salucci, and A. Massa, "Holographic smart EM skins for advanced beam power shaping in next generation wireless environments," *IEEE J. Multiscale Multiphysics Comput. Tech.*, vol. 6, pp. 171-182, Oct. 2021.

[7] G. Oliveri, A. Gelmini, A. Polo, N. Anselmi, and A. Massa, "System-by-design multi-scale synthesis of task-oriented reflectarrays," *IEEE Trans. Antennas Propag.*, vol. 68, no. 4, pp. 2867-2882, Apr. 2020.

[8] M. Salucci, L. Tenuti, G. Gottardi, A. Hannan, and A. Massa, "System-by-design method for efficient linear array miniaturisation through low-complexity isotropic lenses" *Electronic Letters*, vol. 55, no. 8, pp. 433-434, May 2019.

[9] M. Salucci, N. Anselmi, S. Goudos, and A. Massa, "Fast design of multiband fractal antennas through a system-by-design approach for NB-IoT applications," *EURASIP J. Wirel. Commun. Netw.*, vol. 2019, no. 1, pp. 68-83, Mar. 2019.

[10] M. Salucci, G. Oliveri, N. Anselmi, and A. Massa, "Material-by-design synthesis of conformal miniaturized linear phased arrays," *IEEE Access*, vol. 6, pp. 26367-26382, 2018.

[11] M. Salucci, G. Oliveri, N. Anselmi, G. Gottardi, and A. Massa, "Performance enhancement of linear active electronically-scanned arrays by means of MbD-synthesized metalenses," *Journal of Electromagnetic Waves and Applications*, vol. 32, no. 8, pp. 927-955, 2018.

[12] G. Oliveri, M. Salucci, N. Anselmi and A. Massa, "Multiscale System-by-Design synthesis of printed WAIMs for waveguide array enhancement," *IEEE J. Multiscale Multiphysics Computat. Techn.*, vol. 2, pp. 84-96, 2017.

[13] A. Massa and G. Oliveri, "Metamaterial-by-Design: Theory, methods, and applications to communications and sensing - Editorial," *EPJ Applied Metamaterials*, vol. 3, no. E1, pp. 1-3, 2016.

[14] G. Oliveri, F. Viani, N. Anselmi, and A. Massa, "Synthesis of multi-layer WAIM coatings for planar phased arrays within the system-by-design framework," *IEEE Trans. Antennas Propag.*, vol. 63, no. 6, pp. 2482-2496, June 2015.

[15] G. Oliveri, L. Tenuti, E. Bekele, M. Carlin, and A. Massa, "An SbD-QCTO approach to the synthesis of isotropic metamaterial lenses" *IEEE Antennas Wireless Propag. Lett.*, vol. 13, pp. 1783-1786, 2014.

[16] A. Massa, G. Oliveri, P. Rocca, and F. Viani, "System-by-Design: a new paradigm for handling design complexity," *8th European Conference on Antennas Propag. (EuCAP 2014), The Hague, The Netherlands*, pp. 1180-1183, Apr. 6-11, 2014.

[17] P. Rocca, M. Benedetti, M. Donelli, D. Franceschini, and A. Massa, "Evolutionary optimization as applied to inverse problems," *Inverse Problems - 25 th Year Special Issue of Inverse Problems, Invited Topical Review*, vol. 25, pp. 1-41, Dec. 2009.

[18] P. Rocca, G. Oliveri, and A. Massa, "Differential Evolution as applied to electromagnetics," *IEEE Antennas Propag. Mag.*, vol. 53, no. 1, pp. 38-49, Feb. 2011.

[19] P. Rocca, N. Anselmi, A. Polo, and A. Massa, "Pareto-optimal domino-tiling of orthogonal polygon phased arrays," *IEEE Trans. Antennas Propag.*, vol. 70, no. 5, pp. 3329-3342, May 2022.

[20] P. Rocca, N. Anselmi, A. Polo, and A. Massa, "An irregular two-sizes square tiling method for the design of isophoric phased arrays," *IEEE Trans. Antennas Propag.*, vol. 68, no. 6, pp. 4437-4449, Jun. 2020.

[21] P. Rocca, N. Anselmi, A. Polo, and A. Massa, "Modular design of hexagonal phased arrays through diamond tiles," *IEEE Trans. Antennas Propag.*, vol.68, no. 5, pp. 3598-3612, May 2020.

[22] N. Anselmi, L. Poli, P. Rocca, and A. Massa, "Design of simplified array layouts for preliminary experimental testing and validation of large AESAs," *IEEE Trans. Antennas Propag.*, vol. 66, no. 12, pp. 6906-6920, Dec. 2018.

[23] N. Anselmi, P. Rocca, M. Salucci, and A. Massa, "Contiguous phase-clustering in multibeam-on-receive scanning arrays," *IEEE Trans. Antennas Propag.*, vol. 66, no. 11, pp. 5879-5891, Nov. 2018.

[24] G. Oliveri, G. Gottardi, F. Robol, A. Polo, L. Poli, M. Salucci, M. Chuan, C. Massagrande, P. Vinetti, M. Mattivi, R. Lombardi, and A. Massa, "Co-design of unconventional array architectures and antenna elements for 5G base station," *IEEE Trans. Antennas Propag.*, vol. 65, no. 12, pp. 6752-6767, Dec. 2017.

[25] N. Anselmi, P. Rocca, M. Salucci, and A. Massa, "Irregular phased array tiling by means of analytic schemata-driven optimization," *IEEE Trans. Antennas Propag.*, vol. 65, no. 9, pp. 4495-4510, Sept. 2017.

[26] N. Anselmi, P. Rocca, M. Salucci, and A. Massa, "Optimization of excitation tolerances for robust beam-forming in linear arrays" *IET Microwaves, Antennas & Propagation*, vol. 10, no. 2, pp. 208-214, 2016.

[27] P. Rocca, R. J. Mailloux, and G. Toso, "GA-Based optimization of irregular sub-array layouts for wideband phased arrays desig," *IEEE Antennas and Wireless Propag. Lett.*, vol. 14, pp. 131-134, 2015.

[28] P. Rocca, M. Donelli, G. Oliveri, F. Viani, and A. Massa, "Reconfigurable sum-difference pattern by means of parasitic elements for forward-looking monopulse radar," *IET Radar, Sonar & Navigation*, vol 7, no. 7, pp. 747-754, 2013.

[29] P. Rocca, L. Manica, and A. Massa, "Ant colony based hybrid approach for optimal compromise sum-difference patterns synthesis," *Microwave Opt. Technol. Lett.*, vol. 52, no. 1, pp. 128-132, Jan. 2010.

[30] P. Rocca, L. Manica, and A. Massa, "An improved excitation matching method based on an ant colony optimization for suboptimal-free clustering in sum-difference compromise synthesis," *IEEE Trans. Antennas Propag.*, vol. 57, no. 8, pp. 2297-2306, Aug. 2009.

[31] N. Anselmi, L. Poli, P. Rocca, and A. Massa, "Design of simplified array layouts for preliminary experimental testing and validation of large AESAs," *IEEE Trans. Antennas Propag.*, vol. 66, no. 12, pp. 6906-6920, Dec. 2018.

[32] M. Salucci, F. Robol, N. Anselmi, M. A. Hannan, P. Rocca, G. Oliveri, M. Donelli, and A. Massa, "S-Band spline-shaped aperture-stacked patch antenna for air traffic control applications," *IEEE Trans. Antennas Propag.*, vol. 66, no. 8, pp. 4292-4297, Aug. 2018.

[33] F. Viani, F. Robol, M. Salucci, and R. Azaro, "Automatic EMI filter design through particle swarm optimization," *IEEE Trans. Electromagnet. Compat.*, vol. 59, no. 4, pp. 1079-1094, Aug. 2017.